ACS APPLIED MATERIALS & INTERFACES

Research Article

Cite This: ACS Appl. Mater. Interfaces 2019, 11, 1040−1048

www.acsami.org

A Few-Minute Synthesis of $CsPbBr_3$ Nanolasers with a High Quality Factor by Spraying at Ambient Conditions

Anatoly P. Pushkarev,*[,†] Viacheslav I. Korolev,[†] Daria I. Markina,[†] Filipp E. Komissarenko,[†] Arnas Naujokaitis,[‡] Audrius Drabavičius,[‡] Vidas Pakštas,[‡] Marius Franckevičius,[‡] Soslan A. Khubezhov,[§] Denis A. Sannikov,[∥,⊥] Anton V. Zasedatelev,[∥] Pavlos G. Lagoudakis,[∥,#] Anvar A. Zakhidov,[†,▽] and Sergey V. Makarov*[,†]

[†]Department of Nanophotonics and Metamaterials, ITMO University, 197101 St. Petersburg, Russia

[‡]Center for Physical Sciences and Technology, LT-10257 Vilnius, Lithuania

[§]Department of Physics, North Ossetian State University, 362025 Vladikavkaz, Russia

[∥]Skolkovo Institute of Science and Technology, 143026 Moscow, Russia

[⊥]P.N. Lebedev Physical Institute of RAS, 119991 Moscow, Russia

[#]University of Southampton, Southampton SO17 1BJ, United Kingdom

[▽]University of Texas at Dallas, Richardson, Texas 75080, United States

Supporting Information

ABSTRACT: Inorganic cesium lead halide perovskite nanowires, generating laser emission in the broad spectral range at room temperature and low threshold, have become powerful tools for the cutting-edge applications in the optoelectronics and nanophotonics. However, to achieve high-quality nanowires with the outstanding optical properties, it was necessary to employ long-lasting and costly methods of their synthesis, as well as postsynthetic separation and transfer procedures that are not convenient for large-scale production. Here we report a novel approach to fabricate high-quality $CsPbBr_3$ nanolasers obtained by rapid precipitation from dimethyl sulfoxide solution sprayed onto hydrophobic substrates at ambient conditions. The synthesis technique allows producing the well-separated nanowires with a broad size distribution of 2−50 μm in 5−7 min, being the fastest method to the best of our knowledge. The formation of nanowires occurs via ligand-assisted reprecipitation triggered by intermolecular proton transfer from $(CH_3)_2CHOH$ to H_2O in the presence of a minor amount of water. The XRD patterns confirm an orthorhombic crystal structure of the as-grown $CsPbBr_3$ single nanowires. Scanning electron microscopy images reveal their regular shape and truncated pyramidal end facets, while high-resolution transmission electron microscopy ones demonstrate their single-crystal structure. The lifetime of excitonic emission of the nanowires is found to be 7 ns, when the samples are excited with energy below the lasing threshold, manifesting the low concentration of defect states. The measured nanolasers of different lengths exhibit pronounced stimulated emission above 13 μJ cm^{-2} excitation threshold with quality factor Q = 1017−6166. Their high performance is assumed to be related to their monocrystalline structure, low concentration of defect states, and improved end facet reflectivity.

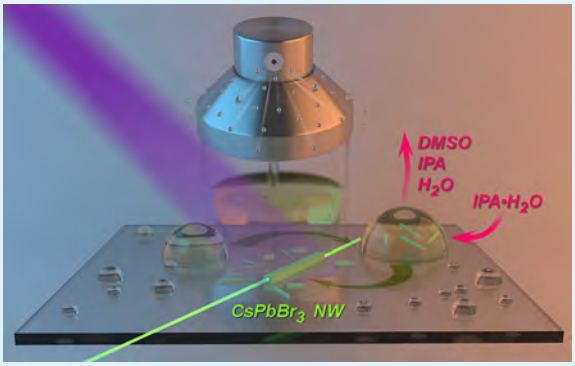

KEYWORDS: *nanolaser, nanowire, lead halide perovskite, $CsPbBr_3$, synthesis, spraying, high Q-factor lasing*

INTRODUCTION

Since the breakthrough reports dedicated to the utilization of $MAPbI_3$ (MA: methylammonium) material for efficient photoconversion in thin-film mesoscopic solar cells,[1,2] the variety of new applications of lead halide perovskites have been discovered. One of the recent cutting-edge applications of these materials is perovskite nanowires (NWs), being much more compact than microplates[3] and generating laser emission in the 420−824 nm range.[4−7] Such NWs alongside with perovskite-based microdisk and microring lasers could serve as a miniature active optical medium for the development of Fabry−Pérot sensors and photonic integrated circuits capable of ultrafast information processing,[8] light-propagation management,[9,10] and photodetection.[11] Although they have already demonstrated lasing with a very low excitation threshold 0.22−40 μJ cm^{-2}, high quality factor (Q = 1500−3600) and short

Received: October 9, 2018
Accepted: December 12, 2018
Published: December 12, 2018

DOI: 10.1021/acsami.8b17396
ACS Appl. Mater. Interfaces 2019, 11, 1040−1048

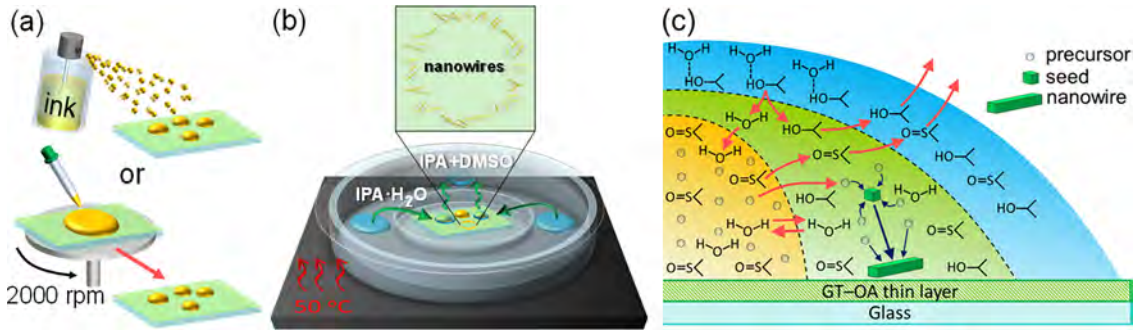

Figure 1. (a) Perovskite precursor ink deposition onto a glass substrate covered with GT-OA mixture thin layer. (b) $CsPbBr_3$ NWs fabrication procedure. (c) Schematic representation of the mechanism of NWs precipitation.

radiative decay (τ = 20−70 ps) in a lasing mode, and certain progress in manufacturing of some advanced devices by top-down lithography has been achieved,[10,11] there is a problem in their facile large-scale fabrication.

The issue related to the production of $CsPbX_3$ (X = Cl, Br, I) nanolasers that are more temperature- and moisture-tolerant, as well as less photodegradable than MA or FA (formamidinium) containing ones, stems from the methods of synthesis presented in the literature. They can be grown as a nanoforest on the surface of a glass/PEDOT:PSS (poly(3,4-ethylenedioxythiophene) polystyrenesulfonate)/PbI_2 thin-film structure immersed in a CsX-methanol (X = Cl, Br, I) solution[6] or by means of chemical vapor deposition (CVD) in an inert atmosphere.[7,12−15] The former method requires the entire growth process to be carried out in a N_2-filled glovebox for 12 h, whereas the latter employs an expensive furnace with controllable gas flow rate. Furthermore, both methods do not allow large-scale fabrication of ordered arrays of nanolasers vital for the photonic chips design and production.

Herein we report on the scalable and cost-effective fabrication of $CsPbBr_3$ nanowires, which can be performed at ambient conditions more than 100 times faster as compared to previously published wet chemical synthesis.[6] We show that perovskite precursor ink can be just sprayed onto an arbitrary substrate (e.g., glass or ITO) covered by a hydrophobic layer, eliminating the problem of substrates selection. Despite the high speed of fabrication, this high-throughput method yields NWs with high-quality walls and end facets, allowing to achieve the record values of the spectral width of lasing modes for NWs-based nanolasers at room temperature (i.e., $Q > 6000$ at wavelength 537.6 nm). Our finding is the next step toward fully integrated, stable, high-quality, and low-cost nanolasers for optoelectronic and nanophotonic applications.[16]

RESULTS AND DISCUSSION

Method of NWs Fabrication. To implement the synthesis of $CsPbBr_3$ nanolasers, we combined a one-step solution self-assembly method with a strategy of substrate surface hydrophobization successfully exploited for the fabrication of $MAPbBr_3$ microdisks.[17,18] First, a solution of $PbBr_2$ (0.3 M) and CsBr (0.3 M) in anhydrous dimethyl sulfoxide (DMSO, 3 mL) was prepared in a N_2-filled glovebox. Then the perovskite precursor ink was poured in a vial with a spray cap (for details, see Figure S1 in the Supporting Information) and taken out from the glovebox. In order to make the substrates surface hydrophobic, Wang et al. polished them with a polyethylene piece,[18] whereas we utilized a fine finishing paste consisting of 100 nm Cr_2O_3 nanoparticles, glyceryl tristearate (GT), and oleic acid (OA). While polishing, tiny Cr_2O_3 grains do not leave noticeable scratches, however, mechanically remove hydrophilic chemical groups from the surface and, therefore, facilitate the spreading of hydrophobic GT and OA over it. The ink was spray-casted onto the substrates to form many separate drops of 0.5−2 mm in diameter (Figure 1a, Figure S1). Importantly, the deposition was carried out at air humidity not exceeding 30% and 20 °C. Alternatively, similar drops can be deposited by spin-coating the preliminary aerated solution (for details, see Methods). After the deposition, the samples were put in a plastic Petri dish bottom placed in a bigger glass one preheated on a hot plate up to 50 °C. Then, 200 μm of hydrous 2-propanol (IPA) was poured in the glass bottom and all the system was capped with a glass dish top. Then, the samples were dried on the hot plate for 5−7 min at 50 °C in the presence of IPA·H_2O vapor (Figure 1b, Figure S1). As a result, equiangularly spaced NWs along with pieces of bulk material inside the circles were precipitated (Figure S2).

According to the observed spatial distribution of the perovskite material, it is reasonable to propose that the synthesis proceeds as follows (see Figure 1c): (i) the azeotropic vapor condenses on the drop of hydrous perovskite precursor ink; (ii) the intermediate layer containing the precursors, H_2O, DMSO, and IPA molecules is formed due to the interdiffusion process; (iii) the concentrations of IPA and H_2O in the intermediate layer become sufficient to initiate the perovskite nucleation; (iv) $CsPbBr_3$ seed crystals build up their crystal lattice by merging $PbBr_2$ and CsBr species; (v) DMSO and IPA molecules diffuse into the outer layer of the drop and volatilize, while aqua ones move to the ink core, saturate it, and invoke the precipitation of the polycrystalline bulk material.

Since polar solvents rapidly decompose lead halide perovskites, the regulation of water molar concentration in the intermediate layer of the drop is a key point in the described synthesis. The water content in both sprayed drops and azeotrope is crucial by reason for H_2O comes to the reaction volume from both the ink core and antisolvent shell. We used 95% azeotrope, whereas the ink drops had been enriched with traces of moisture from 30% humid air before they reached the substrate surface. Pouring of 200 μm of IPA·H_2O into the Petri dish was found not producing the bulk material in the intermediate layer and assisting DMSO to volatilize in 5−7 min. For instance, without azeotropic vapor treatment, the ink drops become dry in 20−25 min and form only bulk polycrystalline precipitate (Figure S3). In addition, to verify the role of water in the synthesis, a similar reaction was conducted in the glovebox by using anhydrous DMSO and IPA solvents. As expected, no NWs were obtained as well.

DOI: 10.1021/acsami.8b17396
ACS Appl. Mater. Interfaces 2019, 11, 1040−1048

Moreover, since the precipitation yet occurs in the presence of a large excess of the hydrous precipitant, it is surprising that the H_2O content in the reaction volume does not achieve a critical value to induce the formation of the bulk $CsPbBr_3$. There appears to be 2-propanol−water separation using a heavy-boiling entrainer (dimethyl sulfoxide)[19] takes part in the regulation of the water content in the intermediate layer. During such extractive distillation, IPA goes overhead and H_2O goes inside the ink core (Figure 1c).

Mechanism of NWs Formation. To gain an insight into the chemistry of NWs formation, we suggest it occurs via ligand-assisted reprecipitation (LARP).[20] 2-Propanol (IPA) is a protic solvent able to reversibly donate a proton to H_2O. Produced H_3O^+ and $[(CH_3)_2CHO]^-$ ions act as capping ligands for $CsPbBr_3$ seed crystals and do not allow them to agglomerate (Scheme 1). The protonated alcohol belongs to

Scheme 1. Synthesis of Nanowires, Nanoplates, or Bulk $CsPbBr_3$ via Water-Mediated Ligand-Assisted Reprecipitation[a]

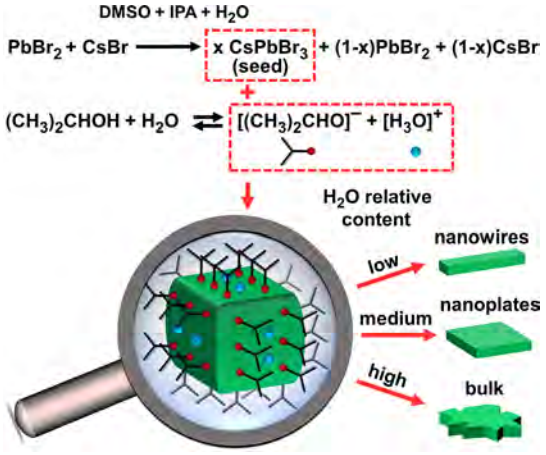

[a]The capping ligands are formed owing to intermolecular proton transfer between 2-propanol and H_2O. Water relative content influences the formation of a resulting reaction product.

the Lewis bases well-known as coordinating to acidic (Pb^{2+} cations) surface sites,[21,22] whereas H_3O^+ species are most likely concentrated at other available sites to maintain a proper charge balance of the seed.[23] Because $CsPbX_3$ nanocrystals are considerably ionic in nature, their interactions with capping ligands are also ionic and labile.[21] The lability is well reflected in dynamic absorption and release of the ligands by the seeds. Annihilation of the released ligands provides the seeds with the opportunity to build up their crystal lattice via in situ crystallization for a short time. Recently, Rogach and co-workers reported on the water-assisted size and shape control of inorganic $CsPbBr_3$ nanocrystals (NCs).[24] In the synthesis, HO^- and H_3O^+ along with OA^- and OLA^+ ions generated by the reaction of water additive with OA and OLA were suggested to be capping ligands. In our case, a minor amount of OA also could come to the reaction volume from the GT-OA thin layer. To ensure there are only two species—H_3O^+ and $[(CH_3)_2CHO]^-$—ruling the growth of nanowires, the same synthesis onto the hydrophobic Si wafer nonpassivated with GT-OA film was additionally conducted. SEM images of the sample confirmed the formation of the NWs around the bulk perovskite (Figure S4).

It is worth noting that, when two or more *core−shell* drops merged on the substrates into one, $CsPbBr_3$ nanoplates were precipitated along with nanowires (Figure S5). Presumably, the drops merging leads to a local increase in the water content, which, in turn, increases the concentration of the capping ligands. It has been proved that the concentration of capping ligands and their nature could significantly affect the size, shape, and phase of perovskite nano-objects to a different extent.[24−26] For example, a reverse trend was revealed for $CsPbBr_3$ NCs synthesized by water-mediated LARP reaction: square-shaped rectangular NCs were isolated using dry toluene and a precursor with 30 μL of water, while 2 times larger additive was sufficient to get nanowires.[24]

The synthesis of $CsPbBr_3$ NWs presented in this work has the following advantages: (i) it utilizes common and cheap chemicals; (ii) it can be conducted at ambient conditions instead of an inert gas atmosphere; (iii) spray-casting makes it large scalable; (iv) the reaction goes more than 100 times faster as compared to the previously reported ones employed for the fabrication of organic−inorganic or inorganic perovskite nanolasers; (v) the final product is separate NWs not requiring further refinement or transfer (Table 1).

Despite that the rapid and highly repeatable synthesis of NWs is achieved for $CsPbBr_3$, the extension of our method to their trichloride and triiodide counterparts turns out to be problematic for our approach. We assume that a compact crystal lattice of $CsPbCl_3$ hampers the attaching of one of the sterically large $[(CH_3)_2CHO]^-$ ions at neighbor Pb^{2+} sites. On the contrary, for $CsPbI_3$, the Pb···Pb distances are large enough to provide free space between two capping anions. Thus, lead atoms are not well shielded from the precursors molecules, which abolishes the formation of nanowires.

Structural Characterization of NWs. Samples for the characterization were prepared employing a slightly modified protocol of the aforementioned synthesis (for details, see Methods) which allows us to isolate nanowires of 2−50 μm length over the large areas. Bright-field optical microscopy images of the samples are presented in Figures 2a and S6. SEM images of single nanowires on the ITO slide showed that almost all of them have the truncated pyramid-shaped end facets (Figure 2b,c and Figure S7), however, the pyramidal and rectangular facets also were found in rare cases (Figure S7). Cross-sectional geometrical parameters for tens of NWs having 1−50 μm length were estimated from high-resolution scanning electron microscopy (HRSEM) images. It was established that the width-to-height ratio lies between 1.1 and 1.5 (Figure S8). The X-ray diffraction (XRD) patterns of the samples collected from the large area using the grazing incidence method exhibited complex signals assigned to overlapping diffraction peaks of orthorhombic and cubic $CsPbBr_3$ phases along with an amorphous halo originating from X-ray scattering from the GT-OA organic layer (Figure 2d). The peaks of the cubic phase, apparently, belong to nano- and microplates (Figure S9) as well as bulk polycrystalline material. In order to solely characterize the NWs, the X-ray beam was collimated to the 100 μm diameter spot and the samples were measured in the $\theta-\theta$ geometry. Six single nanowires located in one plane gave two strong peaks describing diffraction from (110) and (220) crystallographic planes and two weak peaks corresponding to (002) and (004) ones (Figure 2d). The high-resolution spectra are presented in Figure 2e. These four peaks identify an orthorhombic $CsPbBr_3$ (space group *Pbnm*).[28] In this case, the absence of the other sharp lines in the spectrum can be

DOI: 10.1021/acsami.8b17396
ACS Appl. Mater. Interfaces 2019, 11, 1040−1048

Table 1. A Comparative Description of Perovskite NWs Wet Chemical Synthesis

NWs material	chemicals	conditions	synthesis duration (h)	separate NWs	ref
$MAPbCl_xBr_{3-x}$ ($0 \le x \le 1.24$) $MAPbBr_yI_{3-y}$ ($0 \le y \le 3$)	$Pb(AC)_2$, MAX[a], IPA	ambient	20	no	4
$FAPbI_3$, $FAPbBr_3$ $(FA_{0.48}MA_{0.54})PbI_3$ $(FA_{0.71}MA_{0.29})Pb(Br_{2.78}I_{0.22})$ $(FA_{0.67}MA_{0.33})Pb(Br_{2.69}I_{0.31})$	$Pb(AC)_2$, FAX[a], IPA	ambient	20	no	5
$MAPbI_3$	$Pb(AC)_2$, MAX[a], PEDOT:PSS, IPA	ambient	16	no	27
$MAPbBr_3$	$PbBr_2$, MABr, DMF[b], DCM[c]	ambient	24	yes	18
$CsPbX_3$[a]	PbI_2, CsX[a], PEDOT:PSS, MeOH[d], IPA	N_2	12	no	6
$CsPbBr_3$	$PbBr_2$, CsBr, Cr_2O_3, GT, OA, DMSO, IPA	ambient	0.085	yes	this work

[a]X = Cl, Br, I. [b]DMF: *N*,*N*-dimethylformamide. [c]DCM: dichloromethane. [d]MeOH: methanol.

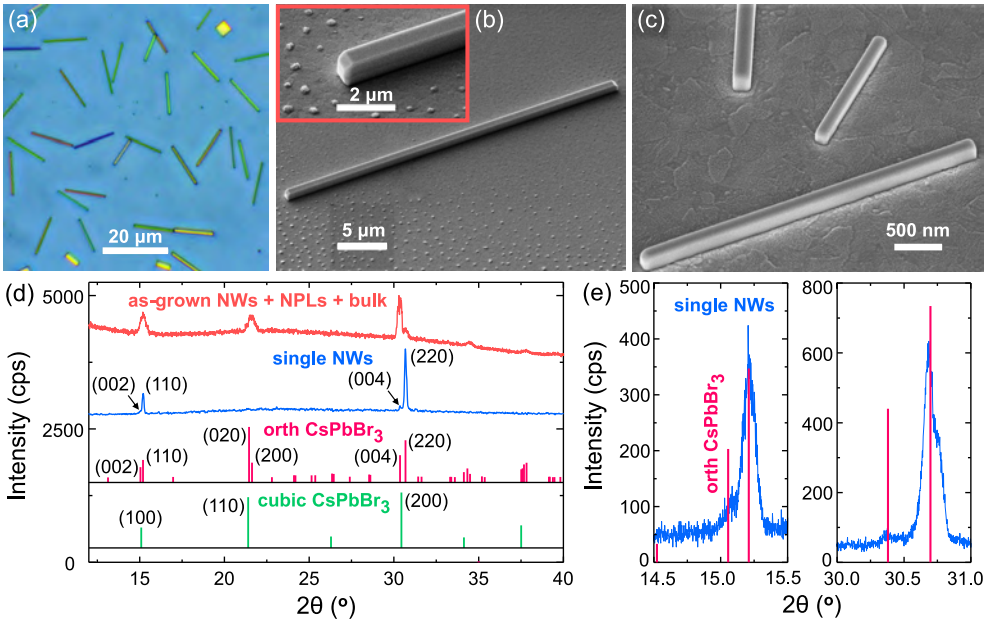

Figure 2. (a) The bright-field image of the separate NWs on ITO substrate. (b) Tilted-view SEM image (45°) of a single nanolaser of 38.5 μm length and the shape of its end facet in the inset picture. (c) High-resolution SEM image of the small NWs. (d) XRD patterns of the sample containing NWs, nanoplates (NPLs), and bulk polycrystalline perovskite on the GT-OA passivated glass slide. The red spectrum was measured from the large surface area, while the blue one was solely collected from NWs using a collimated X-ray beam. An amorphous halo in the red spectrum corresponds to a signal from the GT-OA thin layer. The standard XRD patterns of orthorhombic (orth) and cubic $CsPbBr_3$ are depicted for comparison purposes. (e) High-resolution XRD spectra of the single NWs.

explained by the single-crystal structure of the in-plane grown nanowires. The halo from the organic layer was not observed in the pattern, because DMSO solution washed GT-OA film off the substrate surface locally.

In fact, powder XRD analysis is not sufficient to comprehensively describe the quality of the nanocrystals because of its low sensitivity to minor phases. To reveal the absence of tiny crystalline inclusions and defectless structure, transmission electron microscopy (TEM, Figure 3a), high-resolution TEM, and fast Fourier transform (HRTEM and FFT, Figure 3b) images were acquired from nanowires grown on a TEM grid. The images confirmed monocrystalline NWs having a very low surface roughness (less than 2 nm). These features are vital for nanolasers operation since they affect strongly the lasing threshold and *Q* factors of lasing modes.

Optical Characterization of NWs. Continuous photoluminescence (PL) of NWs was obtained under 360 nm UV lamp excitation (Figure S10). Spontaneous emission with λ_{max} = 525 nm and $\delta\lambda$ = 17 nm (Full Width at Half Maximum, FWHM) was measured from the center of evenly illuminated NWs (Figure 4a, image/spectrum (i)). When NWs were excited with laser beam only at the end facet (Figure 4a, image

DOI: 10.1021/acsami.8b17396
ACS Appl. Mater. Interfaces 2019, 11, 1040−1048

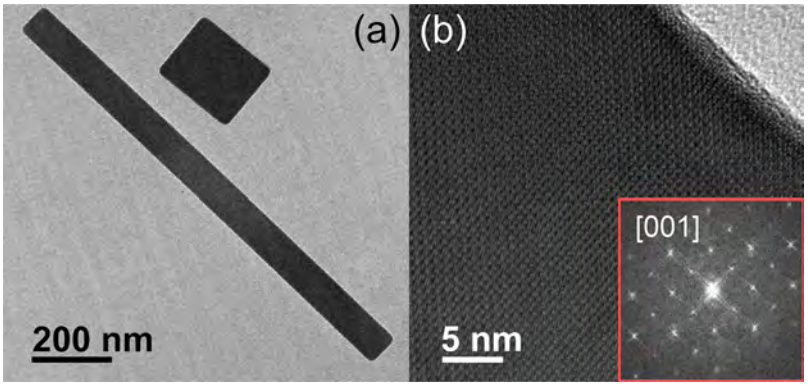

Figure 3. (a) TEM image of a single $CsPbBr_3$ nanowire and a nanoplate grown on a grid. (b) HRTEM and FFT images of the nanowire along the [001] zone axis, confirming its single-crystalline structure.

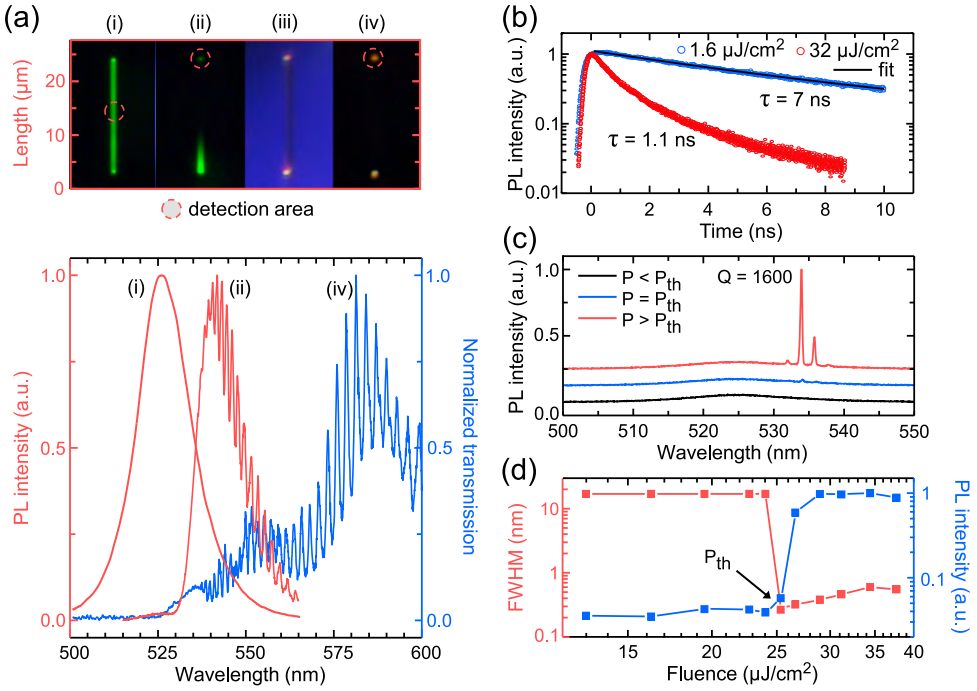

Figure 4. (a) Images of photoluminescence from the center (i) and end facet (ii) of 20.5 μm nanowire, white light transmitted through the NW in the dark-field regime with additional frontal lighting (iii) and without (iv). The spectrum of PL from the edge (ii) is red-shifted (due to the self-absorption of the generated light by the optical resonator medium) with respect to that of the central area (i) and, furthermore, it demonstrates narrow F–P peaks. The same F–P peaks are observed in the transmission spectrum (iv). (b) Spontaneous emission decay of the NWs radiating in the pre- and post-threshold regimes. (c) Multimode laser generation from 11 μm NW. (d) PL intensity and FWHM value versus excitation fluence relationship.

(ii)), the opposite edge emitted red-shifted modulated PL with a smaller FWHM. The bathochromic shift was found to be dependent on the optical path length between the excitation and emission areas and is attributed to partly self-absorbed by the laser medium light propagating inside a Fabry–Pérot (F–P) cavity.[29,30] For instance, a 20.5 μm NW gave the waveguide-confined PL peaked at 540 nm with $\delta\lambda$ = 15 nm (Figure 4a, spectrum (ii)). The multiple sharp peaks originate from the resonance optical transmission of the cavity.[29] The same modulation was found in the transmission spectra collected from the end facet, when the opposite one was illuminated with white light (Figure 4a, image/spectrum (iv)).

To study charge carrier dynamics in the nanowires, we employed a time-resolved photoluminescence technique. Figure 4b shows the PL decay kinetics for two different excitation fluences. When exciting below the lasing threshold, the PL signal decayed monoexponentially with a time constant of about 7 ns which is similar to that observed by Park et al. for $CsPbBr_3$ NWs fabricated by a CVD method.[7] Such PL behavior manifests the negligible charge carrier trapping in the NWs. However, a significant change in the emission lifetime was observed when the excitation density exceeded the lasing threshold. The PL decay became about 1.1 ns. The observed lifetime shortening was expectedly due to the bimolecular recombination of the generated free charge carriers. According to the previous measurements with high time resolution,[6,30] stimulated emission decay from similar NWs was much shorter (down to tens of ps), which is less than the resolution of our setup (for details, see Methods).

Stimulated emission from the facets of the nanowires was detected after 400 nm femtosecond pulsed laser excitation (see Methods for the experimental details). At excitation fluence

DOI: 10.1021/acsami.8b17396
ACS Appl. Mater. Interfaces 2019, 11, 1040–1048

below the lasing threshold (P_{th}), 11 μm NW showed PL centered at 525 nm linearly enhancing with the fluence. Above the threshold, four sharp peaks at 532, 534, 535.83, and 537.88 nm corresponding to Fabry−Pérot lasing modes sprang up and grew linearly in the 1.1−1.5 P_{th} value range as well (Figure 4c). PL intensity versus incident pump energy relationship demonstrated the "S"-curve character. The FWHM value remained constant (17 nm) below the P_{th}, decreased down to 0.28 nm at the threshold point and increased above it (Figure 4d). The maximum quality factor of a lasing mode in a resonator determined as $Q = \lambda/\delta\lambda$, where λ = 534 nm is the peak center wavelength and $\delta\lambda$ = 0.28 nm is the peak width, was found to be close to 1900. Remarkably, the Q factor was nearly 2 times larger than that of similar $CsPbBr_3$ NW with a rectangular cross section fabricated by an already developed wet chemical method (Q = 1009).[6] Such enhancement can be explained in terms of improved end facets reflectivity, since according to the quality factor for the F−P resonator $Q_{FP} = Lk_{\|}/\ln|r_1r_2|$, where r_1 and r_2 are the reflection coefficients at each facet, L is the nanowire length, and $k_{\|}$ is wavenumber along the nanowire axis. The higher the reflectivity, the larger Q_{FP} factor. According to our full-wave numerical simulations (see Figure S11 in the Supporting Information), the reflectivity (out-coupling efficiency) of NWs with truncated pyramidal end facets is much less that those for rectangular facets. Indeed, the tapered shape of a waveguide traps light in the vicinity of the very end owing to oblique incidence of light.[31] Also, more narrower lasing mode comes from the reduced surface roughness and bulk defects, because total quality factor (Q_{tot}) of a resonator consists of the contributions from them as well. As a result, according to the Schawlow−Townes equation: $\delta\lambda \sim Q_{tot}^{-2}$, it is clear that the spectral width of the lasing mode in nanowires tends to be minimal for the best nanowires quality.

The mode spacing between the laser peaks varies with the NW length as $\Delta\lambda = (\lambda^2/2n_gL)$, where n_g is a group refractive index. The latter was reported to be 6−7 times larger[7] than that of bulk $CsPbBr_3$ (n = 2.3) and inversely dependent on NW length.[29] To estimate n_g, we measured the lasing from three lasers with lengths 4.3 (NW **1**), 10.5 (NW **2**), and 22.5 μm (NW **3**) at 1.2P_{th} excitation pump (Figure 5). The thresholds were in the 13−100 μJ cm^{-2} range. Lineshape analysis of the laser lines revealed that **1** generated two-mode emission consisting of peaks perfectly matching the Gaussian function, whereas every peak of **2** and **3** fitted a double-Gaussian distribution manifesting that both nanolasers gave two sets of lasing modes (Figure 5). From the mode spacing equal to 4.95, 2.15, and 1.1 nm, the n_g values 6.76, 6.38, and 5.86 were calculated for **1**, **2**, and **3**, respectively. Careful inspection of the dependence of the mode spacing on reciprocal length for numerous as-grown nanolasers showed a linear trend from which an average value $\bar{n}_g \approx 7.5$ was derived (Figure S12). On the contrary, the quality factor of the lasing modes increased with the length and achieved 6166 (at 1.2P_{th}) and 6542 (at P_{th}) for 22.5 μm nanowire. To the best of our knowledge, these values are record among those mentioned in the literature for the rest of lead halide perovskite NWs.

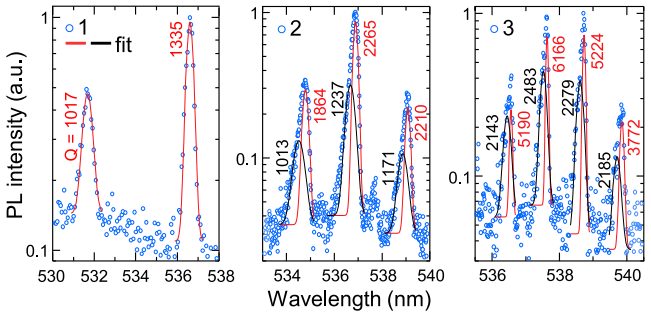

Figure 5. Q-factor analysis for the nanowires **1** (4.3 μm), **2** (10.5 μm), and **3** (22.5 μm) selected to demonstrate lasing at 1.2P_{th} fluence. Gaussian (for **1**) and double-Gaussian (for **2** and **3**) fitting of the laser lines. FWHM values of the laser modes with the highest quality factor equal to 0.4, 0.237, and 0.087 nm for NWs **1**−**3**, respectively (at P_{th} excitation, the corresponding modes are somewhat narrower—0.334, 0.197, and 0.082 nm—and have larger Q factor - 1598, 2724, and 6542).

The quality factor of an optical resonator suffers from two types of losses. The first one—radiative losses—includes an escape of the confined light through the end facet mirrors and its scattering by the volume or surface defects. The second one is nonradiative losses originating from charge carriers relaxation via trap states and self-absorption of the generated light by the laser medium. In our NWs, the radiative dissipation is minimized owing to improved end facet reflectivity confirmed by full-wave numerical simulation as well as monocrystalline structure and smooth surface morphology proved by transmission electron microscopy. The absence of the volume defects was additionally confirmed by dark-field microscopy proving no scattering from the internal area of the nanowires (Figure 4a, Figure S13). The main reason for nonradiative losses stems from the charge carrier trap states. The initially low concentration of such states in the as-prepared NWs was verified by using time-resolved spectroscopy. They can be produced by H_2O impurities in the perovskite structure. Although water traces were demonstrated to be not affecting the structural integrity of perovskite NCs and even enhancing their photoluminescence,[24] the H_2O presence can cause the Pb^{2+} hydroxylation destroying the $[PbBr_6]^{4-}$ octahedral species and thus produce the charge carriers trapping sites. Nevertheless, it seems this degradation process is not rapid since photophysical properties of the synthesized $CsPbBr_3$ NWs kept at ambient conditions for a month remained virtually unchanged.

Achievement of high-Q lasing from F−P micro- and nanoresonators is challenging; however, it makes it possible to design optical sensors capable of detection of various analytes at ultralow concentrations. In this term, high Q factor is a crucial parameter, because the larger number of times a photon undergoes internal reflection or recirculation, the more pronounced its interaction with analyte molecules via an evanescent optical field that extends from the sensor surface and decays exponentially with distance.[32,33] Another one cutting edge application—photonic integrated circuits—requires integration of high-Q nanolasers arrays with silicon to engineer, for instance, a high-speed multichannel coherent transmitter[8] operating at extremely low channel spacing. In this regard, perovskite NWs are promising candidates, since they are compatible with silicon and can be grown as arrays by a nanopatterned PDMS (polydimethylsiloxane) template-confined synthesis.[34] Such $MAPbBr_3$ nanowires arrays demonstrated lasing with Q = 500 due to their polycrystalline structure. We assume combining the presented few-minute synthesis and the template-assisted fabrication strategy will open up new perspectives in the development of both high-

DOI: 10.1021/acsami.8b17396
ACS Appl. Mater. Interfaces 2019, 11, 1040−1048

quality perovskite-based optical sensors and photonic integrated circuits.

CONCLUSION

In summary, we have developed a rapid synthesis of high-quality $CsPbBr_3$ perovskite nanolasers, which proceeds as follows: Drops of the perovskite precursor ink deposited on the substrate surface by spraying at ambient conditions react with 2-propanol−water azeotropic vapor to give separate nanowires with a broad size distribution of 2−50 μm in 5−7 min. The formation of nanowires (NWs) occurs in the perovskite precursors-containing DMSO−IPA·H_2O medium via ligand-assisted reprecipitation triggered by the reversible intermolecular proton transfer between $(CH_3)_2CHOH$ and H_2O species in the presence of a minor amount of water. The water content in the reaction volume is assumed to be regulated owing to IPA−water separation using a heavy-boiling entrainer (DMSO). The XRD patterns of the single NWs confirmed they are orthorhombic crystals which, according to HRTEM and FFT images, possess superior structural integrity and smooth surface morphology. Their regular shape and truncated pyramidal end facets were observed in the SEM images. Slow monoexponential spontaneous emission decay (τ = 7 ns) proved the negligible charge carrier trapping in the NWs. The nanolasers of 4.3−22.5 μm lengths showed lasing above the 13−100 μJ cm^{-2} excitation threshold with Q = 1017−6166. Obviously, their high performance is specified by their monocrystalline structure, low concentration of defect states, and improved end facet reflectivity. Since the presented synthesis allows very fast cost-effective and large-scale fabrication of high-performance nanolasers, we believe it will open up new perspectives in the development of perovskite-based optical sensors and photonic integrated circuits.

METHODS

Materials. Lead(II) bromide ($PbBr_2$, 99.999%, Alfa Aesar), cesium bromide (CsBr, 99.999%, Sigma-Aldrich), dimethyl sulfoxide (DMSO, anhydrous, 99.8%, Alfa Aesar), isopropyl alcohol (IPA, technical grade, 95%, Vecton), oleic acid (OA, technical grade, 90%, Vecton), chromium(III) oxide (Cr_2O_3 nanopowder, <100 nm particle size (TEM), 98%, Sigma-Aldrich), and glyceryl tristearate (stearin, technical grade, Sigma-Aldrich) were used as received.

Preparation of Finishing Composite. Cr_2O_3 (0.700 g), glyceryl tristearate (0.150 g), and OA (0.150 g) were added to a ceramic mortar, heated up to 100 °C in an oven, homogenized by a pestle, and cooled down to room temperature to give a dark green paste.

Preparation of Perovskite Solution. $PbBr_2$ (0.110 g, 0.3 mmol) and CsBr (0.0636 g, 0.3 mmol) were added to a 5 mL glass vial and dissolved in DMSO (3 mL) by shaking for 10 min to afford a clear solution. Then the solution was filtered by using a 0.45 μm syringe adapter with a PTFE membrane. The chemicals were stored and mixed inside a N_2-filled glovebox with both O_2 and H_2O levels not exceeding 1 ppm.

$CsPbBr_3$ Nanowires Fabrication. Glass, ITO, and hydrophobic silicon substrates were purchased from commercial suppliers. Glass and ITO substrates were polished with the chromium oxide paste and rinsed with distilled water to ensure the surface of substrates was evenly hydrophobic. Hydrophobic Si plates were used as received. Two methods of perovskite solution deposition onto the substrates were used. In the first case, the perovskite ink was poured in a vial with a spray cap and taken out from the glovebox. Then the $CsPbBr_3$ solution was immediately spray-casted onto a substrate located at a distance of 40 cm from the vial to form many separate drops of 0.5−2 mm in diameter. In the second case, the prepared perovskite solution was taken out from the glovebox, exposed to humid air (30%) for a minute, and kept in the closed vial for 15 min. Then 20 μL of the perovskite ink was dripped onto a rotating substrate in 2 s when the rotation speed reached the set maximum (2000 rpm) and spun for 30 s. In both cases, the sample was put in a plastic Petri dish bottom (35 × 9 mm) placed in a bigger glass one (80 × 15 mm) preheated on the hot plate up to 50 °C. 200 μm of IPA·H_2O azeotrope was poured in the glass bottom, and all the system was capped with a glass dish top. Thus, the sample was dried on the hot plate for 5−7 min at 50 °C in the presence of 2-propanol−water azeotropic vapor. To prepare the samples containing separate NWs distributed over large areas of the substrates, the azeotropic vapor was allowed to condense on the deposited drops of the perovskite ink and then the drops were merged and spread over the substrate surface without the Petri dish opening.

Characterization. The bright-field and fluorescent images of the samples were obtained by using an Axio Imager A2m (Carl Zeiss) microscope with 10×, 50×, and 100× objectives (Carl Zeiss EC Epiplan-NEOFLUAR). PL spectrum of a single NW was recorded by using an optical fiber spectrometer (Ocean Optics QE Pro) coupled with the microscope in the fluorescent regime. The area of detection was a spot of 2 μm diameter. The absence of the large volume defects in nanolasers was verified by means of dark-field microscopy as follows: nanowires were illuminated at an oblique angle 65° to the normal of the surface by s-polarized light from a halogen lamp (HL2000-FHSA) through a weakly focusing objective (Mitutoyo M Plan Apo NIR, 10×, NA = 0.28). Scattered light was collected from the top by a 50× objective (Mitutoyo M Plan APO NIR, NA = 0.42) and sent to a CCD camera (Cannon 400 D). The transmission spectra of the NWs were measured in the same geometry by using a Horiba LabRam HR spectrometer.

Fluorescence decay kinetics were measured using the Edinburgh Instruments time-correlated single photon counting fluorescence spectrometer F900. The picosecond pulsed diode laser EPL-375 emitting 50 ps pulses at 375 nm with the repetition rate of 20 MHz was used for the sample excitation. The time resolution of the setup was about hundred of picoseconds by applying apparatus function deconvolution. We did not observe any degradation of PL in the longest experiment (the duration was about 10^3 s) carried out at 32 μJ cm^{-2} fluence. From that, the NWs are stable for approximately 1 × 10^{10} laser action cycles.

Morphology and size of the nanowires were studied using a scanning electron microscope (Crossbeam 1540 XB, Carl Zeiss). High-resolution SEM images were obtained on an FE-SEM-FIB HELIOS Nanolab 650 (FEI).

XRD patterns of the nanowires were measured using an X-ray diffractometer SmartLab (Rigaku) equipped with a 9 kW rotating Cu anode X-ray tube. The measurements were performed using the grazing incidence (GIXRD) method in the 2θ range of 10−75°. The angle between the X-ray primary beam and the specimen surface was adjusted to 0.5°. The XRD patterns of single NWs were recorded in the θ−θ geometry on an XRD-7000 diffractometer (Shimadzu) equipped with a 2 kW rotating Cu anode tube, beam collimator and optical microscope. The X-ray beam was collimated to the 100 μm diameter spot, and the measurements were carried out in the scan range 2θ = 10−60° with 0.002° precision.

HRTEM and FFT images were obtained on an FEI Tecnai F20 X-TWIN transmission electron microscope with a field emission gun. Sample measurements were carried-out using the bright-field regime, acceleration tension set for 200 kV, images recorded using a Gatan Orius CCD camera.

Lasing properties of single NWs were studied under nonresonant optical excitation at a wavelength of 400 nm using frequency doubled 180 fs pulses at 1 kHz repetition rate from a high energy Ti:sapphire regenerative amplifier system (Coherent Libra-HE). The beam was focused onto the sample surface at normal incidence by a 4× microscope objective (Nikon Plan Fluor 4X) that was aligned to ensure uniform irradiation of the NWs (Gaussian distribution with an FWHM of 70 μm). Emission of a single rod was collected in transmission configuration using a 100× infinity corrected microscope objective (Mitutoyo Plan Apo 100×) with a numerical aperture NA = 0.5 and focused into a 750 mm spectrometer (Princeton Instruments SP2750) equipped with a cooled electron multiplying CCD camera

DOI: 10.1021/acsami.8b17396
ACS Appl. Mater. Interfaces 2019, 11, 1040−1048

(Princeton Instruments ProEM 1024BX3). The residual light from the excitation beam was blocked by a 473 nm long-pass filter (Semrock RazorEdge LP473). Lasing emission from a single NW was studied by using a 1200 grooves/mm grating (for 0.03 nm spectral resolution) or 300 grooves/mm grating (for 0.12 nm spectral resolution) and a slit width of 20 μm at the entrance of the spectrometer. All measurements were performed at room temperature in air.

■ ASSOCIATED CONTENT

Supporting Information

The Supporting Information is available free of charge on the ACS Publications website at DOI: 10.1021/acsami.8b17396.

Process of the nanowires deposition; bright-field, dark-field, fluorescent optical images, SEM images of the perovskite NWs, nanowires height and width distribution versus their length, full-wave numerical simulations of NW with different end facets, mode spacing versus reciprocal length relationship for as-grown nanolasers (PDF)

■ AUTHOR INFORMATION

Corresponding Authors

*E-mail: anatoly.pushkarev@metalab.ifmo.ru (A.P.P.).
*E-mail: s.makarov@metalab.ifmo.ru (S.V.M.).

ORCID

Anatoly P. Pushkarev: 0000-0002-1793-6812
Sergey V. Makarov: 0000-0002-9257-6183

Notes

The authors declare no competing financial interest.

■ ACKNOWLEDGMENTS

A.P.P. thanks the Russian Science Foundation (grant no. 18-73-00346) for the financial support of NWs synthesis. S.V.M. thanks the Ministry of Education and Science of the Russian Federation (project 14.Y26.31.0010) for optical characterization and calculations. S.A.K. thanks the Ministry of Education and Science of the Russian Federation (project no. 16.9284.2017/7.8) for the support of XRD characterization. A.V.Z., D.A.S. and P.G.L. acknowledge support from the NGP MIT-Skoltech.

■ REFERENCES

(1) Lee, M. M.; Teuscher, J.; Miyasaka, T.; Murakami, T. N.; Snaith, H. J. Efficient Hybrid Solar Cells Based on Meso-Superstructured Organometal Halide Perovskites. *Science* **2012**, *338*, 643−647.

(2) Kim, H.-S.; Lee, C.-R.; Im, J.-H.; Lee, K.-B.; Moehl, T.; Marchioro, A.; Moon, S.-J.; Humphry-Baker, R.; Yum, J.-H.; Moser, J. E.; Grätzel, M.; Park, N.-G. Lead Iodide Perovskite Sensitized All-Solid-State Submicron Thin Film Mesoscopic Solar Cell with Efficiency Exceeding 9%. *Sci. Rep.* **2012**, *2*, 591.

(3) Zhang, Q.; Su, R.; Liu, X.; Xing, J.; Sum, T. C.; Xiong, Q. High-Quality Whispering-Gallery-Mode Lasing from Cesium Lead Halide Perovskite Nanoplatelets. *Adv. Funct. Mater.* **2016**, *26*, 6238−6245.

(4) Zhu, H.; Fu, Y.; Meng, F.; Wu, X.; Gong, Z.; Ding, Q.; Gustafsson, M. V.; Trinh, M. T.; Jin, S.; Zhu, X. Lead Halide Perovskite Nanowire Lasers with Low Lasing Thresholds and High Quality Factors. *Nat. Mater.* **2015**, *14*, 636.

(5) Fu, Y.; Zhu, H.; Schrader, A. W.; Liang, D.; Ding, Q.; Joshi, P.; Hwang, L.; Zhu, X.; Jin, S. Nanowire Lasers of Formamidinium Lead Halide Perovskites and their Stabilized Alloys with Improved Stability. *Nano Lett.* **2016**, *16*, 1000−1008.

(6) Eaton, S. W.; Lai, M.; Gibson, N. A.; Wong, A. B.; Dou, L.; Ma, J.; Wang, L.-W.; Leone, S. R.; Yang, P. Lasing in Robust Cesium Lead Halide Perovskite Nanowires. *Proc. Natl. Acad. Sci. U. S. A.* **2016**, *113*, 1993−1998.

(7) Park, K.; Lee, J. W.; Kim, J. D.; Han, N. S.; Jang, D. M.; Jeong, S.; Park, J.; Song, J. K. Light−Matter Interactions in Cesium Lead Halide Perovskite Nanowire Lasers. *J. Phys. Chem. Lett.* **2016**, *7*, 3703−3710.

(8) Summers, J.; Vallaitis, T.; Evans, P.; Ziari, M.; Studenkov, P.; Fisher, M.; Sena, J.; James, A.; Corzine, S.; Pavinski, D.; Ou-Yang, J.; Missey, M.; Gold, D.; Williams, W.; Lai, M.; Welch, D.; Kish, F. Monolithic InP-Based Coherent Transmitter Photonic Integrated Circuit with 2.25 Tbit/s Capacity. *Electron. Lett.* **2014**, *50*, 1150−1152.

(9) Cegielski, P. J.; Neutzner, S.; Porschatis, C.; Lerch, H.; Bolten, J.; Suckow, S.; Kandada, A. R. S.; Chmielak, B.; Petrozza, A.; Wahlbrink, T.; Giesecke, A. L. Integrated Perovskite Lasers on a Silicon Nitride Waveguide Platform by Cost-Effective High Throughput Fabrication. *Opt. Express* **2017**, *25*, 13199−13206.

(10) Wang, S.; Liu, Y.; Li, G.; Zhang, J.; Zhang, N.; Xiao, S.; Song, Q. Lead Halide Perovskite Based Microdisk Lasers for On-Chip Integrated Photonic Circuits. *Adv. Opt. Mater.* **2018**, *6*, 1701266.

(11) Zhang, N.; Sun, W.; Rodrigues, S. P.; Wang, K.; Gu, Z.; Wang, S.; Cai, W.; Xiao, S.; Song, Q. Highly Reproducible Organometallic Halide Perovskite Microdevices based on Top-Down Lithography. *Adv. Mater.* **2017**, *29*, 1606205.

(12) Zhou, H.; Yuan, S.; Wang, X.; Xu, T.; Wang, X.; Li, H.; Zheng, W.; Fan, P.; Li, Y.; Sun, L.; Pan, A. Vapor Growth and Tunable Lasing of Band Gap Engineered Cesium Lead Halide Perovskite Micro/Nanorods with Triangular Cross Section. *ACS Nano* **2017**, *11*, 1189−1195.

(13) Oksenberg, E.; Sanders, E.; Popovitz-Biro, R.; Houben, L.; Joselevich, E. Surface-Guided CsPbBr3 Perovskite Nanowires on Flat and Faceted Sapphire with Size-Dependent Photoluminescence and Fast Photoconductive Response. *Nano Lett.* **2018**, *18*, 424−433.

(14) Shoaib, M.; Zhang, X.; Wang, X.; Zhou, H.; Xu, T.; Wang, X.; Hu, X.; Liu, H.; Fan, X.; Zheng, W.; Yang, T.; Yang, S.; Zhang, Q.; Zhu, X.; Sun, L.; Pan, A. Directional Growth of Ultralong $CsPbBr_3$ Perovskite Nanowires for High-Performance Photodetectors. *J. Am. Chem. Soc.* **2017**, *139*, 15592−15595.

(15) Wang, X.; Zhou, H.; Yuan, S.; Zheng, W.; Jiang, Y.; Zhuang, X.; Liu, H.; Zhang, Q.; Zhu, X.; Wang, X.; Pan, A. Cesium Lead Halide Perovskite Triangular Nanorods as High-Gain Medium and Effective Cavities for Multiphoton-Pumped Lasing. *Nano Res.* **2017**, *10*, 3385−3395.

(16) Makarov, S.; Furasova, A.; Tiguntseva, E.; Hemmetter, A.; Berestennikov, A.; Pushkarev, A.; Zakhidov, A.; Kivshar, Y. Halide-Perovskite Resonant Nanophotonics. *Adv. Opt. Mater.* **2018**, 1800784.

(17) Liao, Q.; Hu, K.; Zhang, H.; Wang, X.; Yao, J.; Fu, H. Perovskite Microdisk Microlasers Self-Assembled from Solution. *Adv. Mater.* **2015**, *27*, 3405−3410.

(18) Wang, K.; Sun, W.; Li, J.; Gu, Z.; Xiao, S.; Song, Q. Unidirectional Lasing Emissions from CH3NH3PbBr3 Perovskite Microdisks. *ACS Photonics* **2016**, *3*, 1125−1130.

(19) Arifin, S.; Chien, I.-L. Design and Control of an Isopropyl Alcohol Dehydration Process via Extractive Distillation using Dimethyl Sulfoxide as an Entrainer. *Ind. Eng. Chem. Res.* **2008**, *47*, 790−803.

(20) Zhang, F.; Zhong, H.; Chen, C.; Wu, X.-g.; Hu, X.; Huang, H.; Han, J.; Zou, B.; Dong, Y. Brightly Luminescent and Color-Tunable Colloidal CH3NH3PbX3 (X= Br, I, Cl) Quantum Dots: Potential Alternatives for Display Technology. *ACS Nano* **2015**, *9*, 4533−4542.

(21) De Roo, J.; Ibanez, M.; Geiregat, P.; Nedelcu, G.; Walravens, W.; Maes, J.; Martins, J. C.; Van Driessche, I.; Kovalenko, M. V.; Hens, Z. Highly Dynamic Ligand Binding and Light Absorption Coefficient of Cesium Lead Bromide Perovskite Nanocrystals. *ACS Nano* **2016**, *10*, 2071−2081.

(22) Huang, H.; Raith, J.; Kershaw, S. V.; Kalytchuk, S.; Tomanec, O.; Jing, L.; Susha, A. S.; Zboril, R.; Rogach, A. L. Growth Mechanism of Strongly Emitting CH3NH3PbBr3 Perovskite Nanocrystals with a Tunable Bandgap. *Nat. Commun.* **2017**, *8*, 996.

DOI: 10.1021/acsami.8b17396
ACS Appl. Mater. Interfaces 2019, 11, 1040−1048

(23) Geng, C.; Xu, S.; Zhong, H.; Rogach, A. L.; Bi, W. Aqueous Synthesis of Methylammonium Lead Halide Perovskite Nanocrystals. *Angew. Chem., Int. Ed.* **2018**, *57*, 9650.
(24) Zhang, X.; Bai, X.; Wu, H.; Zhang, X.; Sun, C.; Zhang, Y.; Zhang, W.; Zheng, W.; Yu, W. W.; Rogach, A. L. Water-Assisted Size and Shape Control of CsPbBr3 Perovskite Nanocrystals. *Angew. Chem.* **2018**, *130*, 3395−3400.
(25) Sun, S.; Yuan, D.; Xu, Y.; Wang, A.; Deng, Z. Ligand-Mediated Synthesis of Shape-Controlled Cesium Lead Halide Perovskite Nanocrystals via Reprecipitation Process at Room Temperature. *ACS Nano* **2016**, *10*, 3648−3657.
(26) Saidaminov, M.; Mohammed, O.; Bakr, O. Low-Dimensional-Networked Metal Halide Perovskites: The Next Big Thing. *ACS Energy Letters* **2017**, *2*, 889−896.
(27) Yu, H.; Ren, K.; Wu, Q.; Wang, J.; Lin, J.; Wang, Z.; Xu, J.; Oulton, R. F.; Qu, S.; Jin, P. Organic−Inorganic Perovskite Plasmonic Nanowire Lasers with a Low Threshold and a Good Thermal Stability. *Nanoscale* **2016**, *8*, 19536−19540.
(28) Rodová, M.; Brožek, J.; Knížek, K.; Nitsch, K. Phase Transitions in Ternary Caesium Lead Bromide. *J. Therm. Anal. Calorim.* **2003**, *71*, 667−673.
(29) Zhang, S.; Shang, Q.; Du, W.; Shi, J.; Wu, Z.; Mi, Y.; Chen, J.; Liu, F.; Li, Y.; Liu, M.; Zhang, Q.; Liu, X. Strong Exciton−Photon Coupling in Hybrid Inorganic−Organic Perovskite Micro/Nanowires. *Adv. Opt. Mater.* **2018**, *6*, 1701032.
(30) Wang, X.; Shoaib, M.; Wang, X.; Zhang, X.; He, M.; Luo, Z.; Zheng, W.; Li, H.; Yang, T.; Zhu, X.; Ma, L.; Pan, A. High-Quality In-Plane Aligned CsPbX3 Perovskite Nanowire Lasers with Composition Dependent Strong Exciton-Photon Coupling. *ACS Nano* **2018**, *12*, 6170−6178.
(31) Kuchmizhak, A. A.; Kulchin, Y. N.; Vitrik, O. B.; Savchuk, A. G.; Makarov, S. V.; Kudryashov, S. I.; Ionin, A. A. Optical Apertureless Fiber Microprobe for Surface Laser Modification of Metal Films with sub-100 nm Resolution. *Opt. Commun.* **2013**, *308*, 125−129.
(32) Vollmer, F.; Arnold, S. Whispering-Gallery-Mode Biosensing: Label-Free Detection down to Single Molecules. *Nat. Methods* **2008**, *5*, 591.
(33) Luchansky, M. S.; Washburn, A. L.; Martin, T. A.; Iqbal, M.; Gunn, L. C.; Bailey, R. C. Characterization of the Evanescent Field Profile and Bound Mass Sensitivity of a Label-Free Silicon Photonic Microring Resonator Biosensing Platform. *Biosens. Bioelectron.* **2010**, *26*, 1283−1291.
(34) Liu, P.; He, X.; Ren, J.; Liao, Q.; Yao, J.; Fu, H. Organic−Inorganic Hybrid Perovskite Nanowire Laser Arrays. *ACS Nano* **2017**, *11*, 5766−5773.

DOI: 10.1021/acsami.8b17396
ACS Appl. Mater. Interfaces 2019, 11, 1040−1048